Original Research

Effect of Thulium in Bismuth-Boro-Tellurite glass system on radiation shielding parameters using Xcom, Phy-X/PSD, and NgCAL software

Nor Falihan Ramli [1,2], Azuraida Amat [2,*], Nur Arina Mat Rusni [1,2], Wan Yusmawati Wan Yusoff [2], Hasnimulyati Laoding [3]

[1] Faculty of Defence Science and Technology, Universiti Pertahanan Nasional Malaysia, Kem Sungai Besi, 57000 Kuala Lumpur;

[2] Physics Department, Centre for Defence Foundation Studies, Universiti Pertahanan Nasional, Malaysia, Kem Sungai Besi, 57000 Kuala Lumpur, Malaysia;

[3] Faculty of Applied Sciences, Universiti Teknologi Mara Pahang, 26400 Jengka, Pahang, Malaysia

***** Correspondence: azuraida@upnm.edu.my,

Received: January 13, 2025; Accepted: February 28, 2026

Abstract: This article reports the influence of thulium oxide, Tm_2O_3 on radiation shielding parameters of $\{[(B_2O_3)_{0.25}(TeO_2)_{0.75}]_{0.75}\ [(Bi_2O_3)_{0.25}]\}_{1-x}\ [Tm_2O_3]_x$ glass system. The Xcom, Phy-X, and NgCal software are specialized tools designed to evaluate the radiation shielding properties: mass attenuation coefficient, half value layer, mean free path, atomic cross-section, electronic cross-section, effective atomic number, and effective electron density. The radiation performance of the bismuth-boro-tellurite glass reaches its best when the Tm_2O_3 is at 0.030 mol%. The incorporation of thulium significantly improves the glass network density and enhances the gamma-ray attenuation ability, suggesting its potential as an efficient and eco-friendly radiation shielding material.

Keywords: radiation shielding, thulium oxide, mass attenuation coefficient, mean free path.

1. Introduction

The attenuation of gamma radiation by glass materials has attracted considerable interest from researchers in investigating their radiation shielding properties qualities of glasses. The growing utilization of high-energy ionizing radiations, especially gamma rays, across various scientific and technological domains has led to the emergence of radioactive pollution, posing multiple radiation hazards to both humans and the environment. Radiation safety and protection techniques must be developed to keep radiation at safe and acceptable levels and to reduce the effects of radiation exposure. High radiation exposure can lead to radiation sickness as well as long-term health issues like cardiovascular disease and cancer [1]. To reduce the radiation to safe and appropriate levels, a high-quality shielding material is needed. Clay bricks, concrete blocks, and tiles are common materials used for radiation protection. Theoretically, each material with a specific density can function as a shielding material and reduce radiation intensity.

Three computational software tool- Xcom, Phy-X and NgCal were used in this study to theoretically assess the radiation shielding properties. The Xcom program was developed by [2] and its function is to calculate mass attenuation coefficients for any compound, element, and

combination at energies ranging from 1 keV to 100 GeV. Xcom could compute attenuation coefficients for a standard energy grid or a user-specified grid. The development of Photon Shielding and Dosimetry (PSD) software, also referred as Phy-X is an online platform developed for the theoretical evaluation of photon interaction and shielding parameter such as mass attenuation coefficient (MAC), mean free path (MFP) and half value layer (HVL) across a wide energy spectrum. Its user-friendly interface and comprehensive calculation capability motivated its use in present work. While, NgCal was developed for narrow beam transmission properties to ensure theoretical estimates of shielding properties of elements, composites subjected to thermal, and compounds, fast neutrons, and photons with energy of X-rays and gamma rays ranging from 0.002 MeV to 20 MeV. The developed software provides for additional data input in the form of elements /compounds/oxides and their fractions, as well as an explanation of multiple shielding results required by researchers and scientists working on the radiation shielding properties of multi-component materials [3]. Identifying the interaction of radiation emitted, the absorption and attenuation of gamma energy in materials, and analyze the parameters that determine the effectiveness of a material's shielding. Hence, the determination of linear attenuation coefficient (LAC), mass attenuation coefficient (MAC), half-value layer (HVL), tenth-value layer (TVL), mean free path (MFP), effective atomic number (Z_{eff}), effective electron density (N_{el}) is crucial in order to develop suitable shielding materials. A great shielding glass provides complete safety for persons who operate in potentially hazardous environments, such as nuclear power plants or hospital X-ray rooms, by combining high shielding capabilities and resistance against radiation exposure.

Traditionally, many radiation shielding materials include glasses rely on lead-based component due to the high atomic number and density of lead, which make it highly effective in attenuation ionizing radiation. Higher atomic number (Z) or heavy metal oxide concentration in glass allows for enhanced radiation shielding properties. However, lead toxicity possesses a serious environmental and health concern due to its harmful effect on the human body. According to the findings, glasses with bismuth content are a potential alternative to conventional radiation shielding. These types of glasses also serve several purposes being gamma radiation absorbent, transparent to visible light, and having low melting points [4] . Due to its larger density, greater third-order nonlinear optics susceptibility, and higher refractive index, Bi_2O_3 is suitable to be used as a radiation shield [5].

Borate and tellurite glasses are commonly used as the host matrix among all glasses due to their outstanding properties that are desirable for specific applications [7], [8]. Boro-tellurite glasses produce non-linear optical properties, a high refractive index, and a wide infrared transmission window for different applications [9], [10]. Thulium is one of the rare earth ions that is particularly fascinating since it can have significant spectroscopic properties like a fluorescence that is quite sensitive to the environment where the Tm^{3+} ions are located [11], [12]. The choice of the host depends on a variety of factors, including thermal stability, lower phonon energy, etc., that varied between different host matrices. The host has a significant impact on the rare earth ions' luminescence properties [13]. Based on the previous studies tellurite glass system with higher levels of thulium doping significantly enhance its radiation shielding efficiency. This improvement is reflected by a higher linear attenuation coefficient together with reduced half-value layer and mean free path, demonstrated better shielding performance compared to Er_2O_3 and Ho_2O_3 modified glasses as well as other rare-earth doped system [14], [15], [16]. In line with this observation, several theoretical studies have explored the influence of thulium oxide on the radiation shielding

behaviour of glass materials through computational analyses. In those studies, the mass attenuation coefficient has been obtained using the Xcom software, and the result shown that the incorporation of glass dopant (Tm_2O_3) enhances gamma-ray attenuation and improves the overall radiation shielding performance of the glass system. In addition, the Zeff and Nel were calculated using a comprehensive and consistence set of formula [17]. However, there is still a need for a systematic evaluation of thulium's effect on the radiation shielding parameters of bismuth-boro-tellurite glass system using multiple, well-validated computational tools remains limited.

In this study, a boro-tellurite base glass was chosen as it possesses desirable and distinct traits, such as excellent transparency and efficient shielding against gamma radiation when combined with heavy metal oxide. The addition of bismuth oxide (Bi_2O_3) to the glass modification is expected to further improve its shielding properties. Additionally, thulium oxide (Tm_2O_3), which is a high-density rare-earth element, has been introduced into the glass system and shows promise as a potential substitute for lead.

2. Methodology

The glass system with chemical composition of $\{[(B_2O_3)_{0.25}(TeO_2)_{0.75}]_{0.75}\ [(Bi_2O_3)_{0.25}]\}_{1-x}[Tm_2O_3]_x$ (where x = 0.000, 0.005, 0.010, 0.015, 0.020, 0.025, and 0.030 mol%) successfully prepared by melt quenching technique. Each glass batch was prepared from certified reagent grades of TeO_2 (99.95% purity), B_2O_3 (97.5%), Bi_2O_3 (99.975% purity), and Tm_2O_3 (99.99%) of commercial origin which was manufactured and supplied by Alfa Aesar. The chemicals were firstly mixed and ground repeatedly for 30 minutes in an alumina crucible until became excessively a fine powder substance before being heated at 1000°C for 1 hour. After the batch was completely melted, the molten was poured onto the preheated stainless-steel plate and annealed at 400°C for 1 hour before being allowed to cool down to room temperature. The density of these present samples was determined using the Archimedes principle through precise mass measurement in air and in water, with water used as the immersion medium.

In this study, the shielding parameters are calculated by using three software which is the Xcom, Phy-X, and NgCal software. These programs were used to determine several parameters of thulium-doped bismuth boro-tellurite glass based on the empirical compositions $\{[(B_2O_3)_{0.25}(TeO_2)_{0.75}]_{0.75}\,[(Bi_2O_3)_{0.25}]\}_{1-x}\,[Tm_2O_3]_x$, where x varied from 0.000 to 0.030 mol%.

Theoretical values of the mass attenuation coefficients of mixture or compound have been calculated by Xcom, based on the rule of mixture [2].

$$MAC = \sum_{i} w_i (MAC)_i \tag{1}$$

where $w_i$is the weight fraction of the element and $(MAC)_i$ is the mass attenuation coefficient for the individual elements.

Linear attenuation coefficient (LAC) value can be determined using the following equation [13] where ρ is the density of a glass sample: -

$$LAC = MAC \cdot \rho \tag{2}$$

Half value layer, HVL is the convenient parameter to represent the gamma ray interaction of a material. The HVL is the thickness of a particular material needed to reduce the intensity of the

gamma ray to half of its initial value. The half-value layer value can be calculated by the following relation [14]:

$$HVL = \frac{In\ (2)}{LAC} = \frac{0.693}{LAC} \tag{3}$$

While, mean free path, MFP corresponds to the average distance travelled by a moving particle (atom/molecule/photon) between two consecutive collisions [14]. It can be calculated by using the equation:

$$MFP = \frac{\int_0^\infty te^{(-LAC\cdot t)}dt}{\int_0^\infty e^{(-LAC\cdot t)}dt} = \frac{1}{LAC} \tag{4}$$

Using Avogadro's number, N_A, an atomic weight of a constituent element, A, the weight fraction of element, w and MAC value, one can find the atomic cross-section value with the equation as follows [15].

$$ACS = \frac{MAC}{N_A \sum \frac{w}{A}} \tag{5}$$

Here, the weight fraction of element, w, refers to the number of formula units that can be found by [16]: -

$$w = \frac{n \cdot A}{\sum n \cdot A} \tag{6}$$

Furthermore, the electronic cross-section can be found using equation (7) [16]: -

$$ECS = \frac{1}{N_A}\left(\sum \frac{f \cdot A}{Z_i} \cdot (MAC)\right) \tag{7}$$

Where f, Z, Z_{eff} are the fraction of abundance of an element i with respect to the number of atoms such that $f1+f2+f3+\ldots$. $fi=1$, Zi is the atomic number of the ith element, atomic number of element and effective atomic number respectively.

The effective atomic number, Z_{eff} refer to how effectively the glass can interact with or absorb radiation based on its element composition and it can be calculate using the above equation.

$$Z_{eff} = \frac{ACS}{ECS} \tag{8}$$

The electron density, N_{el} can be defined as the number of electrons per unit mass, and it can be mathematically written as follows [14]:

$$N_{el} = \frac{MAC}{ECS} \tag{9}$$

3. Results and discussion

3.1. Raman spectroscopy

Raman spectroscopy is a laser on a material and observing how the light interacts with the atoms inside it. Most of the light bounces back unchanged, but a very small part changes its energy. Figure 1 shows the obtained Raman spectrum for $\{[(B_2O_3)_{0.25}(TeO_2)_{0.75}]_{0.75}\ [(Bi_2O_3)_{0.25}]\}_{1-x}[Tm_2O_3]_x$ glass at different thulium concentrations. At the low-frequency region (~200-500 cm^{-1}) is dominated by a near 400-450 cm^{-1}, first band at 415 cm^{-1} which can be assigned to Te-O-Te bending modes in TeO_4 trigonal bipyramidal and TeO_3 trigonal pyramidal units that form the tellurite network, the shift left

to a lower value of wavenumber is due to the formation of Te-O-Bi and Bi-O-Bi structural units consistent with assignment in rare-earth doped boro-tellurite glass [22], [23], [24]. In the mid-frequency region (~500-800 cm^{-1}), the intense band around 650-750 cm^{-1} corresponds to Te-O stretching vibrations in TeO_4 and TeO_3 units and Te-O-Te linkages, which is typically the most prominent Raman feature in boro-tellurite glass [22], [25], [26]. The high-frequency band (~1200-1500 cm^{-1}) observed near 1300-1400 cm^{-1} is attributed to B-O stretching in BO_3 triangular units associated with the borate component of the glass [22], [27]. With increasing Tm^{3+} concentration, the systematic decreased in intensity of the main tellurite band, together with a nearly constant peak position, indicates that Tm^{3+} behaves predominantly as a network-modifying ions: it weakens Te-O-Te linkages, promotes conversion of TeO_4 to TeO_3 units, and increases the population on non-bridging oxygens (NBOs) leading to reduced network polymerization while preserving the basic $TeO_4/TeO_3/BO_3$ structural motif [28], [29], [23], [24]. Overall, the evolution of Raman intensity and the background with Tm^{3+} content reflects a transition from a more connected tellurite network toward a depolymerized structure enriched in NBOs, in agreement with structural trends deduced from spectroscopy and modelling studies on Tm-doped bismuth boro-tellurite glass.

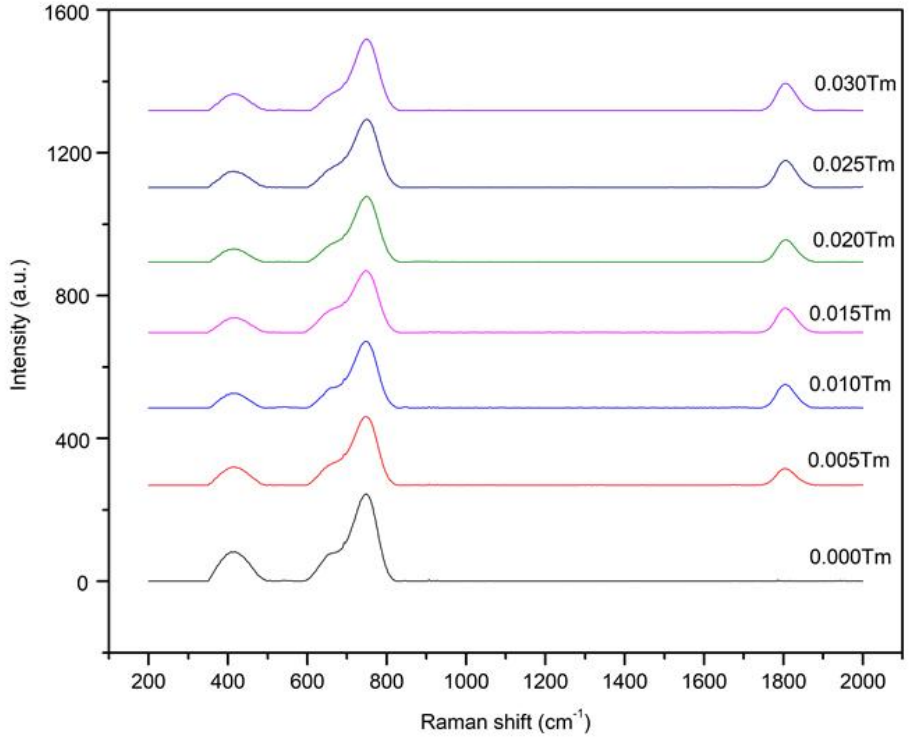

Figure 1. Raman Spectrum of $\{[(B_2O_3)_{0.25}(TeO_2)_{0.75}]_{0.75}[(Bi_2O_3)_{0.25}]\}_{1-x}[Tm_2O_3]_x$ glasses

3.2. Density

The densities and the chemical compositions of each glass sample with different concentrations of Tm_2O_3 of the studied glasses were respectively reported in Table 1. In the present bismuth-boro-tellurite system, the addition of Tm_2O_3 up to 0.030 mol%, the density of the glass system increased from 6.066 g/cm^3 to 6.308 g/cm^3. The increased in density upon Tm_2O_3 doping might be attributed to the higher molecular weight of thulium oxide compared to other chemical oxides [30]. The presence of thulium in the glass network increased the total molecular weight from 219.31 g/cm^3 to 269.28 g/cm^3 material. The density of the glass was also increased since density is directly proportional to molar mass [3], [31]. The previous research [32] also reported that the

density of thulium-doped barium tellurite glass system increased depending on their parameters such as interstitial lattice spacing, coordinator number, and the higher atomic mass of the rare-earth dopant. Another contributing factor to the observed increase in density of these samples are denser packing arrangement of atoms and the consequent structural rearrangement of the glass network caused by the incorporation of the rare-earth oxide [3], [31].

Table 1. Glass code, molar fraction of Tm_2O_3, density and glass composition of present glass samples

Glass code	Molar fraction of Tm_2O_3, x	Density g/cm^3	Glass Composition
0Tm	0.000	6.07	$\{[(B_2O_3)_{0.25}(TeO_2)_{0.75}]_{0.75}(Bi_2O_3)_{0.25}\}_1$
0.005Tm	0.005	6.08	$\{[(B_2O_3)_{0.25}(TeO_2)_{0.75}]_{0.75}(Bi_2O_3)_{0.25}\}_{0.95}(Tm_2O_3)_{0.05}$
0.010Tm	0.010	6.09	$\{[(B_2O_3)_{0.25}(TeO_2)_{0.75}]_{0.75}(Bi_2O_3)_{0.25}\}_{0.90}(Tm_2O_3)_{0.10}$
0.015Tm	0.015	6.11	$\{[(B_2O_3)_{0.25}(TeO_2)_{0.75}]_{0.75}(Bi_2O_3)_{0.25}\}_{0.85}(Tm_2O_3)_{0.15}$
0.020Tm	0.020	6.18	$\{[(B_2O_3)_{0.25}(TeO_2)_{0.75}]_{0.75}(Bi_2O_3)_{0.25}\}_{0.80}(Tm_2O_3)_{0.20}$
0.025Tm	0.025	6.27	$\{[(B_2O_3)_{0.25}(TeO_2)_{0.75}]_{0.75}(Bi_2O_3)_{0.25}\}_{0.75}(Tm_2O_3)_{0.25}$
0.030Tm	0.030	6.31	$\{[(B_2O_3)_{0.25}(TeO_2)_{0.75}]_{0.75}(Bi_2O_3)_{0.25}\}_{0.70}(Tm_2O_3)_{0.30}$

3.2. Mass attenuation coefficient and linear attenuation coefficient

The theoretical values of the mass attenuation coefficient, MAC of $\{[(B_2O_3)_{0.25}(TeO_2)_{0.75}]_{0.75}[(Bi_2O_3)_{0.25}]\}_{1-x}[Tm_2O_3]_x$ glass system is obtained in the energy range of 1keV-100GeV using Xcom, Phy-X, and NgCal as shown in Figure 2. The mass attenuation coefficient generally decreases as the energy of the energy of the incident radiation increases across all glass codes. This trend is expected because higher energy photons are typically less likely to be absorbed or scattered by the material. The addition of Thulium (Tm) dopants seems to have a minor effect on to the MAC at lower energies (0.662 MeV). The values remain relatively consistent, showing little variation across different dopant concentrations. For higher energies, (1.173 MeV and 1.332 MeV), the values are also stable with slight fluctuations, indicating that the dopant content does not significantly alter the attenuation characteristics in this energy range. When comparing the results from the different software tools (Xcom, Phy-X, and NgCal), there is a close agreement in the calculated values, suggesting reliability and consistency in the methods used for evaluating the MAC. The result from Xcom and Phy-X shows similar trends, with slight variations likely due to difference in the underlying algorithms or databases used in the calculations. The MAC for the undoped glass (0Tm) and glasses with varying Tm concentrations are quite close, particularly at 0.662 MeV, with values around 0.0837 cm^2/g.

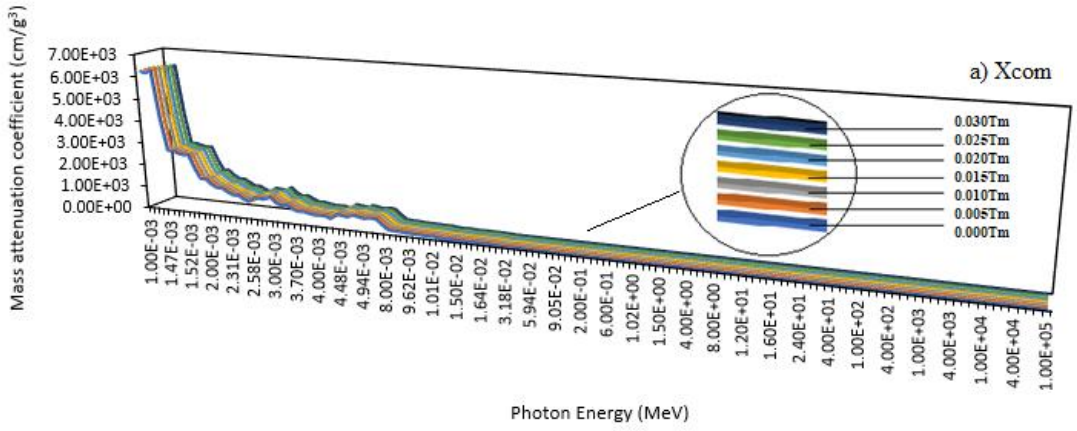

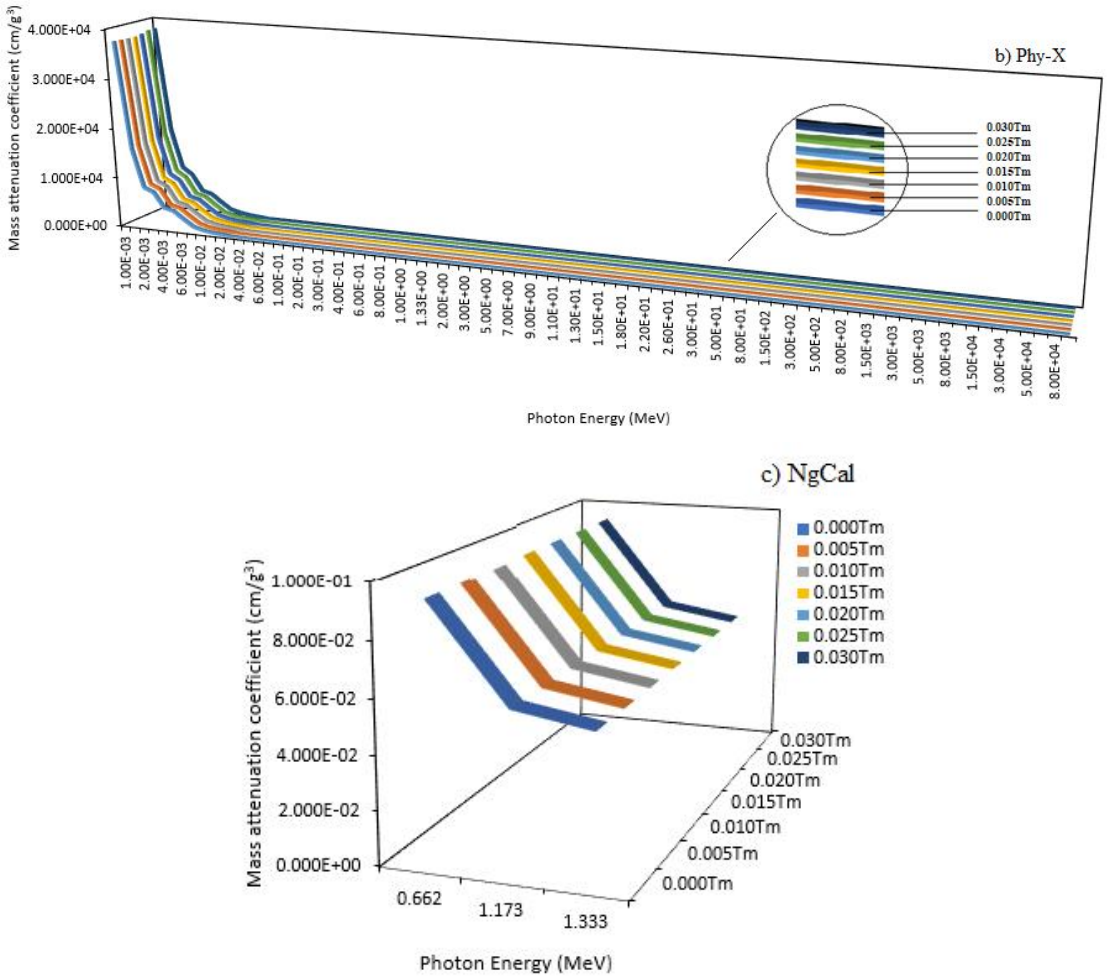

Figure 2. Graph mass attenuation coefficients of present glasses using a) Xcom, b) Phy-X, and c) NgCal

From Table 2, the MAC values increase as thulium oxide, Tm_2O_3 concentration increases. The glass sample 0.030Tm (with a composition of 0.030 mol% of Tm_2O_3) displays the highest MAC in the energy range of 1keV-100GeV. Previously, Xcom was used to study the MAC of various concentrations of thulium oxide (0.1-2.0 mol%) in multicomponent borosilicate glasses with 0.015-5 MeV energy range with 10% Li_2O or MgO. Compared to other glass samples, the 2.0 mol% Tm_2O_3-doped glasses exhibited greater gamma-ray attenuation properties. This indicates that with the addition of Tm_2O_3, photons with higher energy can penetrate the glass samples more easily, whereas low-energy photons are more effectively shielded by the prepared glass [33]. Meanwhile, Phy-X was used to study the mass attenuation coefficient (MAC) for various concentrations of samarium. As the Sm_2O_3 concentration increased, the MAC values decreased, while the density values increased. This behaviour may be explained by the increased contribution of the high-density element samarium to the glass samples and the corresponding reduction in the contribution of the boron component. [34]. In the energy range between 0.356 and 0.662 MeV, the MAC values decrease slightly as the photon energy increases, and the dominance of Compton scattering [35]. The value of MAC is reduced exponentially with increasing photon energy up to 7 MeV and almost constant thereafter, and this is expected according to Beer Lambert's adsorption law. At higher photon energies, the MAC values are very small, indicating that as the photon energy increases, photons can penetrate the glass samples more easily.

At photon energy of 0.662 MeV, the mass attenuation coefficient (MAC) values obtained in the present work using the Xcom software within the range of 0.08373-0.08379 cm^2/g, which are slightly

lower values compared with some previously reports results. For comparison, Alshamari et al. (2023) reported MAC value range of 0.048-0.089 cm^2/g, while W. Cheewasukhanont et al. (2022) obtained values between 0.08728 -0.08899 cm^2/g at the same photon energy using Xcom [47], [51]. These differences can be attributed to variation in glass compositions, density, and rare-earth dopant concentration. Nevertheless, the close agreement between the present results and previously reported data confirms the reliability and validity of the current theoretical calculations.

Table 2 The theoretical values of the mass attenuation coefficient, $\boldsymbol{MAC}$ of Xcom, Phy-X, and NgCal $\{[(B_2O_3)_{0.25}(TeO_2)_{0.75}]_{0.75}[(Bi_2O_3)_{0.25}]\}_{1-x}[Tm_2O_3]_x$ glass system at a photon energy of 0.662, 1.173, and 1.332 MeV.

Glass code	Mass attenuation coefficient, MAC (cm^2/g)								
	Xcom			Phy-X			NgCal		
	0.662 MeV	1.173 MeV	1.333 MeV	0.662 MeV	1.173 MeV	1.333 MeV	0.662 MeV	1.173 MeV	1.333 MeV
0Tm	0.08373	0.05614	0.05207	0.093097	0.058143	0.053522	0.093589	0.058313	0.053668
0.05Tm	0.08363	0.05614	0.05207	0.093071	0.058134	0.053515	0.093554	0.058300	0.053657
0.010Tm	0.08360	0.05612	0.05207	0.093045	0.058125	0.053509	0.093557	0.058298	0.053655
0.015Tm	0.08361	0.05612	0.05207	0.093019	0.058117	0.053502	0.093505	0.058284	0.053644
0.020Tm	0.08373	0.05614	0.05208	0.092993	0.058108	0.053495	0.093505	0.058280	0.053641
0.025Tm	0.08373	0.05614	0.05208	0.092968	0.058100	0.053489	0.093455	0.058267	0.053631
0.030Tm	0.08379	0.05615	0.05209	0.092943	0.058092	0.053482	0.093455	0.058264	0.053628

The linear attenuation coefficient for all the gamma energy increased with the addition of Tm_2O_3 composition as shown in Table 3. It is well known that the radiation shielding efficiency of a material depends on its density. When compared with other studies [36, 37], the LAC values were found to increase at lower photon energies due to the dominance of the photoelectric absorption mechanism. Thulium-doped glasses exhibited the highest LAC value of 0.375 cm^{-1} at 0.662 MeV for 15 mol% MoO_3-doped boro-tellurite glass [36]. As the gamma photon energy increased, the LAC values showed a significant decrease, which is typical behavior as the interaction gradually shifts from the photoelectric effect to the Compton scattering region. However, a slight and unexpected rise in LAC was observed between 0.1 MeV and 0.3 MeV, which can be attributed to the increasing contribution of Compton interactions in this energy range. At very low photon energy (0.015 MeV), the simulated LAC values increased with the addition of Tm_2O_3, corresponding to the higher molar mass and effective atomic number introduced by the thulium oxide [37].

Table 3. Theoretical value of linear attenuation coefficient, LAC for Xcom, Phy-x, and Ngcal $\{[(B_2O_3)_{0.25}(TeO_2)_{0.75}]_{0.75}[(Bi_2O_3)_{0.25}]\}_{1-x}[Tm_2O_3]_x$ glass system with different Tm_2O_3 concentration at a photon energy of 0.662, 1.173, and 1.332 MeV.

Glass code	Linear attenuation coefficient, cm^{-1}								
	Xcom			Phy-X			NgCal		
	0.662 MeV	1.173 MeV	1.333 MeV	0.662 MeV	1.173 MeV	1.333 MeV	0.662 MeV	1.173 MeV	1.333 MeV
0Tm	0.50791	0.34055	0.31592	0.56473	0.35269	0.32466	0.56771	0.35373	0.32555

0.05Tm	0.50805	0.34105	0.31633	0.56541	0.35316	0.32511	0.56834	0.35417	0.32597
0.010Tm	0.50921	0.34183	0.31716	0.56674	0.35404	0.32592	0.56986	0.35509	0.32681
0.015Tm	0.51119	0.34312	0.31836	0.56872	0.35533	0.32711	0.57169	0.35635	0.32798
0.020Tm	0.51754	0.34700	0.32191	0.57479	0.35917	0.33065	0.57795	0.36023	0.33156
0.025Tm	0.52499	0.35200	0.32654	0.58291	0.36429	0.33538	0.58596	0.36534	0.33627
0.030Tm	0.52855	0.35419	0.32858	0.58628	0.36644	0.33737	0.58951	0.36753	0.33829

3.3. Half-value layer and mean free path

The gamma shielding efficiency can also be described in terms of the half-value layer, HVL and mean free path, MFP. To generate a radiation shielding material that is more effective, lower HVL values are required. The half-value layer is the thickness of a material that is required to absorb half of the incident radiation. Meanwhile, the mean free path is the average distance travelled the by photon between two subsequent interactions. The theoretical values of half value layer and mean free path of $\{[(B_2O_3)_{0.25}(TeO_2)_{0.75}]_{0.75}\ [(Bi_2O_3)_{0.25}]\}_{1-x}\ [Tm_2O_3]_x$ glass system is obtained in the energy range of 1keV-100GeV using Xcom, Phy-X, and NgCal as shown in Fig. 2 and Fig. 3. Across all photon energy ranges, the half value layer (HVL) and mean free path (MFP) gradually decreased with increasing Tm_2O_3 content up to 0.030 mol%, as presented in Tables 4 and 5, respectively. This decreasing trend of HVL and MFP for the $\{[(B_2O_3)_{0.25}(TeO_2)_{0.75}]_{0.75}[(Bi_2O_3)_{0.25}]\}_{1-x}[Tm_2O_3]_x$ glass system can be attributed to the enhanced density and mass attenuation coefficient resulting from the incorporation of thulium oxide. The present findings reveal that the 0.030Tm glass exhibits a lower HVL compared to the $SrO–B_2O_3–TeO_2–BaO–MoO_3$ glass reported by [37], indicating its superior photon attenuation capability [26]. Similarly, the 0.030Tm glass demonstrated the lowest MFP compared to the $50BaO–xBi_2O_3–(50–x)$ glass system [38], with corresponding values of 2.84, 4.21, and 4.62 cm at photon energies of 0.662 MeV, 1.173 MeV, and 1.333 MeV, respectively. The gradual increase in MFP with rising photon energy is attributed to the dominance of the Compton scattering process, in which the scattering probability is directly influenced by the atomic number (Z) through the interaction cross-section [39].

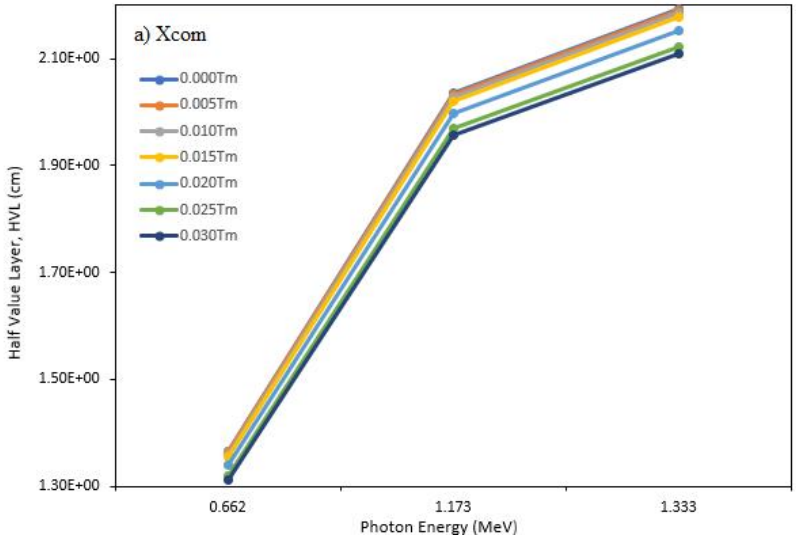

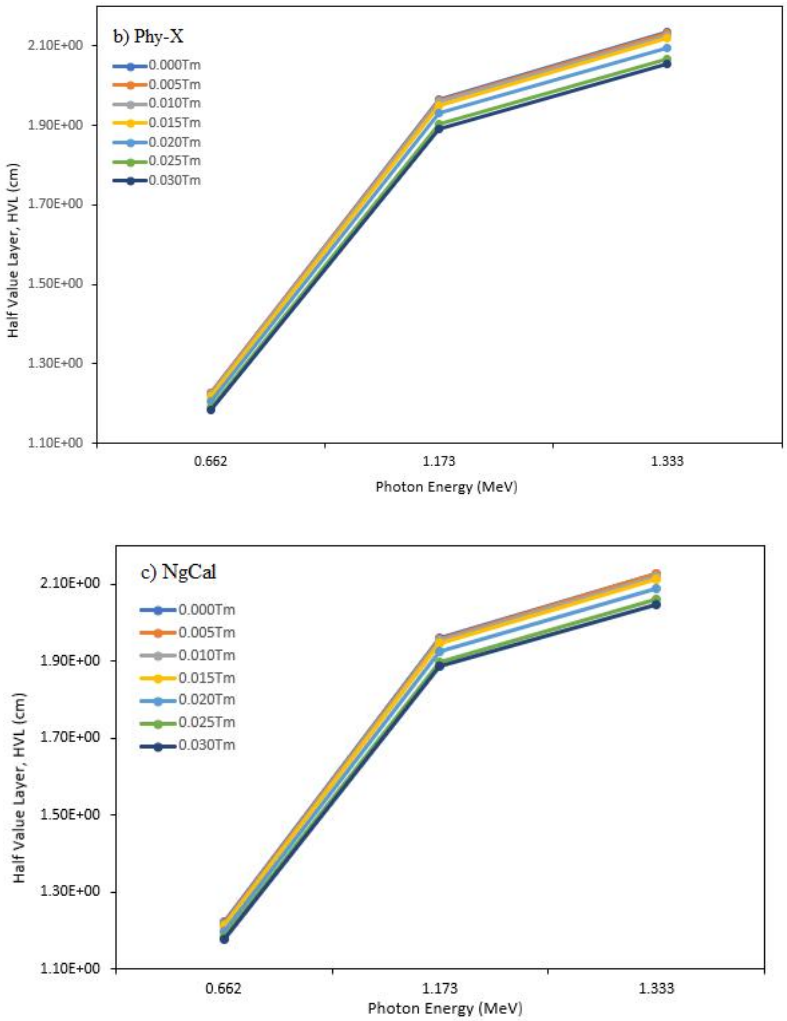

Figure 3. Graph half value layer Tm-doped borotellurite glass using a) Xcom, b) Phy-X, and c) NgCal

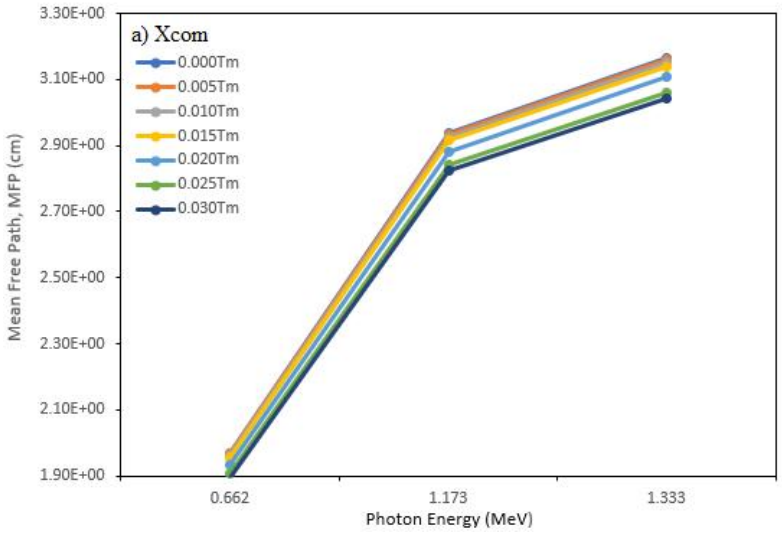

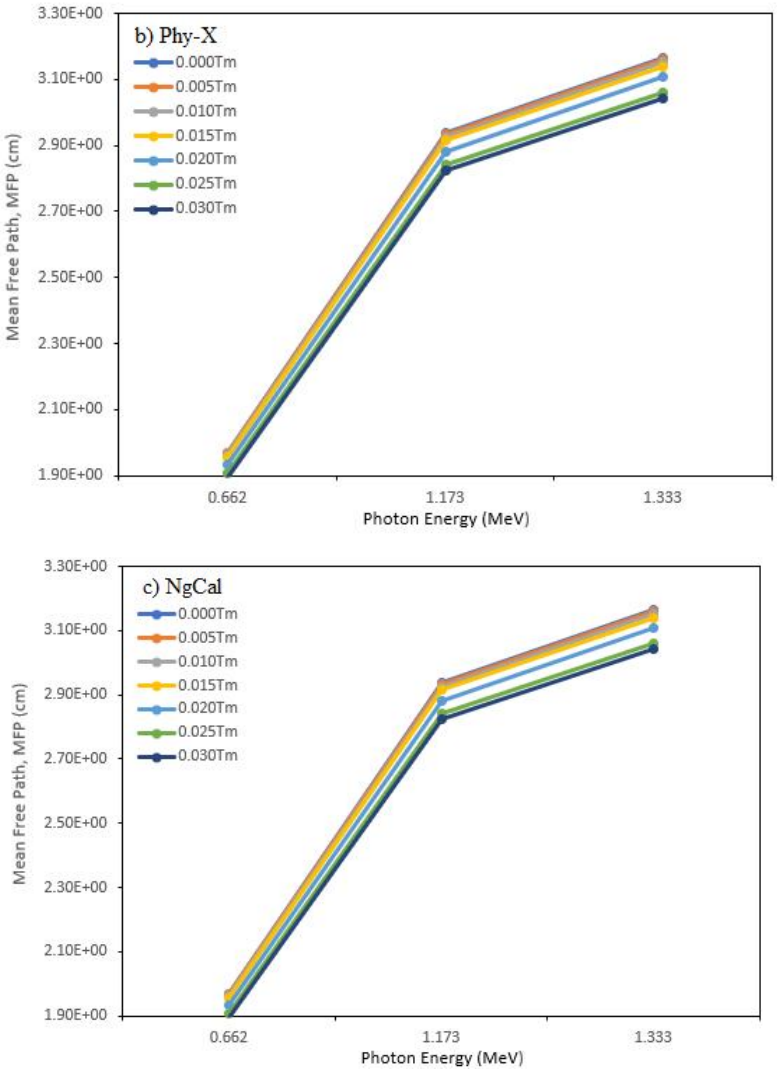

Figure 4. Graph mean free path Tm-doped borotellurite glass using a) Xcom, b) Phy-X, and c) NgCal

Table 4. Theoretical value of half value layer, HVL for Xcom, Phy-X, and Ngcal of present glasses with different Tm_2O_3 concentration at a photon energy of 0.662, 1.173, and 1.332 MeV.

Glass code	Half-value layer (for Photons), cm								
	Xcom			Phy-X			NgCal		
	0.662 MeV	1.173 MeV	1.333 MeV	0.662 MeV	1.173 MeV	1.333 MeV	0.662 MeV	1.173 MeV	1.333 MeV
0Tm	1.3644	2.0350	2.1936	1.2274	1.9653	2.1350	1.2210	1.9595	2.1292
0.05Tm	1.3640	2.0320	2.1908	1.2259	1.9627	2.1321	1.2196	1.9571	2.1264
0.010Tm	1.3609	2.0273	2.1850	1.2230	1.9578	2.1267	1.2164	1.9520	2.1209
0.015Tm	1.3557	2.0197	2.1768	1.2188	1.9507	2.1190	1.2125	1.9451	2.1134
0.020Tm	1.3390	1.9971	2.1528	1.2059	1.9299	2.0963	1.1993	1.9242	2.0906
0.025Tm	1.3200	1.9688	2.1222	1.1891	1.9028	2.0668	1.1829	1.8973	2.0613
0.030Tm	1.3111	1.9566	2.1091	1.1823	1.8916	2.0546	1.1758	1.8860	2.0490

Table 5. Theoretical value of mean free path, MFP for Xcom, Phy-x, and NgCal of present glasses with different Tm_2O_3 concentration at a photon energy of 117, 133, and 662 keV.

Glass code	Mean free path (for Photons), cm								
	Xcom			Phy-X			NgCal		
	0.662 MeV	1.173 MeV	1.333 MeV	0.662 MeV	1.173 MeV	1.333 MeV	0.662 MeV	1.173 MeV	1.333 MeV
0Tm	1.9689	2.9365	3.1654	1.7708	2.8353	3.0801	1.7615	2.8270	3.0717
0.05Tm	1.9683	2.9321	3.1613	1.7686	2.8315	3.0759	1.7595	2.8235	3.0678
0.010Tm	1.9638	2.9255	3.1530	1.7645	2.8245	3.0682	1.7548	2.8162	3.0599
0.015Tm	1.9562	2.9145	3.1411	1.7583	2.8143	3.0571	1.7492	2.8063	3.0489
0.020Tm	1.9322	2.8818	3.1065	1.7398	2.7842	3.0243	1.7302	2.7760	3.0161
0.025Tm	1.9048	2.8409	3.0624	1.7155	2.7451	2.9817	1.7066	2.7372	2.9738
0.030Tm	1.8920	2.8233	3.0434	1.7057	2.7289	2.9641	1.6963	2.7209	2.9561

3.5. Atomic cross section and electronic cross section

Table 6 shows the atomic cross section, ACS of thulium doped borotellurite glass. All the ACS results from Xcom, Phy-X and NgCal are in the order of 10^{-24} cm^2. According to Koirala et al, (2021) [41], ACS provides information on radiation scattering when photons interact with or strike atoms. Since scattering is an important factor in nuclear physics, theoretical analysis of ACS enables the understanding of target material without actually making physical contact. Based on the energy of photons, either coherent scattering, Compton scattering, and photoelectric absorption may occur [40] . Gamma ray photon absorption is favoured by high ACS values. Xcom, Phy-X and NgCal exhibit similar ACS pattern, with ACS being high at low gamma energies and low at high gamma energies. Interaction probability is highest at low energies due to dominant photoelectric absorption, decreased in the intermediate Compton region, and become influenced by pair production at higher energies [41], [32]. Additionally, it is seen that the ACS rises as Tm_2O_3 concentration does as well. This demonstrates that there is significant scattering, which denotes strong photon divergence and increases shielding against gamma ray energy. According to the findings, the suggested glass 0.030Tm is the best radiation shielding material.

Table 6. Calculated atomic cross section of Tm-doped borotellurite glass using Xcom, Phy-X and NgCal software.

Glass Code	Atomic Cross Section (for Photons) ($\times 10^{24}$) (cm^2)								
	Xcom			PhyX			NgCal		
	0.662 MeV	1.173 MeV	1.333 MeV	0.662 MeV	1.173 MeV	1.333 MeV	0.662 MeV	1.173 MeV	1.333 MeV
0.000Tm	7.8691	5.2762	4.8946	8.7496	5.4644	5.0302	8.7826	5.4723	5.0364
0.050Tm	7.8783	5.2886	4.9052	8.7676	5.4764	5.0413	8.8119	5.4913	5.0540
0.010Tm	7.8939	5.2991	4.9167	8.7856	5.4884	5.0524	8.8466	5.5125	5.0735
0.015Tm	7.9133	5.3115	4.9282	8.8035	5.5003	5.0635	8.8472	5.5147	5.0757
0.020Tm	7.9430	5.3257	4.9405	8.8214	5.5122	5.0746	8.8843	5.5375	5.0967
0.025Tm	7.9613	5.3380	4.9519	8.8392	5.5240	5.0856	8.8828	5.5383	5.0976
0.030Tm	7.9853	5.3512	4.9643	8.8569	5.5358	5.0966	8.9202	5.5612	5.1188

Table 7 shows the software Xcom, Phy-X, and NgCal produced ECS that were in the range of 10^{-25} cm^2/g. The tendency of increased ECS as the concentration of Tm_2O_3 increases is seen based on

the data from all software. According to Koirala et al. (2021) [41], a high ECS indicates a high interaction between radiation shielding material and gamma rays, which results in enhance shielding performance. The best recommended glass composition for radiation shielding materials in Xcom, Phy-X and NgCal is 0.030Tm glass which has the highest concentration of Tm_2O_3. This demonstrates the rare earth oxide of Tm_2O_3 has beneficial qualities to be used as radiation shielding glass. In studied energy range, ECS decreased with increasing photon energy in the Compton-dominated region, consistent with photon interaction theory; however, at any fixed energy, ECS increased with Tm_2O_3 content, indicating enhanced electron density and shielding effectiveness. Thus, it can be inferred that at higher gamma energies, photons and radiation shielding material interact more strongly. This claim also is supported by [42].

Table 7. Calculated electronic cross section of Tm-doped borotellurite glass using Xcom, Phy-X and NgCal software

Glass Code	Electronic Cross Section (for Photons) ($\times 10^{24}$) (cm^2/g)								
	Xcom			PhyX			NgCal		
	0.662 MeV	1.173 MeV	1.333 MeV	0.662 MeV	1.173 MeV	1.333 MeV	0.662 MeV	1.173 MeV	1.333 MeV
0.000Tm	2.9910	2.0044	1.8594	2.9155	2.0620	1.9200	3.3358	2.0797	1.9142
0.050Tm	2.9886	2.0038	1.8589	2.9147	2.0618	1.9198	3.3355	2.0796	1.9142
0.010Tm	2.9883	2.0036	1.8587	2.9139	2.0615	1.9196	3.3370	2.0799	1.9143
0.015Tm	2.9836	2.0026	1.8581	2.9131	2.0613	1.9194	3.3367	2.0798	1.9143
0.020Tm	2.9830	2.0025	1.8579	2.9123	2.0611	1.9192	3.3382	2.0801	1.9145
0.025Tm	2.9838	2.0030	1.8578	2.9115	2.0608	1.9190	3.3378	2.0800	1.9144
0.030Tm	2.9869	2.0027	1.8579	2.9107	2.0606	1.9188	3.3387	2.0803	1.9146

3.6. Effective atomic number and effective electron density

The effective atomic number (Z_{eff}), which characterizes the gamma-ray attenuation capability of a radiation shielding material, is one of the key parameters in evaluating its performance as an absorber medium. For practical applications, the proposed thulium-doped borotellurite glass is expected to exhibit a high Z_{eff} value to ensure superior shielding effectiveness. Materials with higher Z_{eff} values tend to attenuate photons more efficiently, as their atomic constituents present a greater probability for photon interactions, thereby increasing the likelihood of collision events [43]. In this study, the 0.030Tm glass exhibited the highest effective atomic number (Z_{eff}), as shown in Table 7, making it the most favorable composition among the proposed glass samples. The Z_{eff} values are strongly influenced by the density of the material, where a higher density generally corresponds to a higher Z_{eff} [44]. Therefore, the higher atomic number and density of the 0.030Tm glass make it reasonable that this composition exhibits the highest Z_{eff} among all the studied samples. Furthermore, the results reveal that Z_{eff} decreases with increasing gamma-ray energy. At higher photon energies, the lower Z_{eff} values indicate that photons are less likely to be absorbed by the target material due to the dominance of the Compton scattering process over the photoelectric effect.

Table 8. Calculated effective atomic number of Tm-doped zinc borotellurite glass using Xcom, Phy-X and NgCal

Glass Code	Effective Atomic Number (for Photons)								
	Xcom			Phy-X			NgCal		
	0.662 MeV	1.173 MeV	1.333 MeV	0.662 MeV	1.173 MeV	1.333 MeV	0.662 MeV	1.173 MeV	1.333 MeV
0.000Tm	26.3453	26.3454	26.3448	30.0597	26.5190	26.2149	26.3054	26.3053	26.3050
0.050Tm	26.4035	26.4033	26.4032	30.1133	26.5740	26.2702	26.4003	26.4004	26.3998
0.010Tm	26.4629	26.4624	26.4637	30.1668	26.6289	26.3253	26.5011	26.5011	26.5003
0.015Tm	26.5191	26.5230	26.5227	30.2200	26.6836	26.3802	26.5147	26.5152	26.5146
0.020Tm	26.5803	26.5806	26.5804	30.2731	26.7381	26.4350	26.6235	26.6238	26.6243
0.025Tm	26.6388	26.6393	26.6388	30.3260	26.7924	26.4896	26.6310	26.6313	26.6304
0.030Tm	26.6977	26.6972	26.6984	30.3788	26.8466	26.5440	26.7408	26.7404	26.7412

A comparative analysis of the effective atomic number (Z_{eff}) was performed to further evaluate the gamma-ray attenuation capability of the prepared glasses. As presented in Table 9, the 0.030Tm glass exhibits a noticeably higher Z_{eff} value compared to several reported radiation shielding materials, including Barium–Magnesium–Sodium–Alumina–Borate glass [45], TeO_2–Na_2O–$NdCl_3$–Sm_2O_3 glass [46], $10Bi_2O_3$–$70B_2O_3$–20BaO glass [47], and $10Bi_2O_3$–$35TeO_2$–$35B_2O_3$–20BaO glass [48]. This enhancement can be attributed to the higher density and the presence of heavy metal oxides such as Bi_2O_3 and Tm_2O_3 in the proposed composition, both of which contribute to an increased effective atomic number and improved photon interaction probability. The higher Z_{eff} value of the 0.030Tm glass therefore suggests its enhanced ability to attenuate gamma radiation, highlighting its strong potential for use as an efficient radiation shielding material in nuclear and medical applications.

Table 9. Comparison between the values of the effective atomic number of the proposed glass(0.030Tm) and other reported shielding materials

Radiation Shielding Material	Effective Atomic Number		
	1.173 MeV	1.332 MeV	0.662 MeV
Barium–Magnesium–Sodium-Alumina- Borate [35]	11.57	11.56	12.06
TeO_2–Na_2O-$NdCl_3$-Sm_2O_3 [36]	-	17.52	-
$10Bi_2O_3$-$70B_2O_3$-20BaO [37]	-	-	15.62
$10Bi_2O_3$-$35TeO_2$-$35B_2O_3$-20BaO [37]	-	-	21.95
0.030Tm Phy-X (Present Work)	30.37881	26.84666	26.54404
0.030Tm NgCal (Present Work)	26.74081	26.74040	26.74120
0.030Tm Xcom (Present Work)	26.69776	26.69727	26.69840

The effective electron density (N_{el}), which represents the number of electrons per unit mass, is another key parameter in evaluating the shielding effectiveness of materials against ionizing radiation. For efficient absorption of gamma photons, a high effective electron density is essential [48]. Table 10 presents the N_{el} values calculated using Xcom, Phy-X, and NgCal software at photon energies of 0.662 MeV, 1.173 MeV, and 1.332 MeV. The results show that N_{el} decreases as the photon

energy increases, following a similar trend to that observed for the mass attenuation coefficient (MAC) and atomic cross-section (ACS). This correlation indicates that N_{el} is directly dependent on MAC and ACS, consistent with the findings reported by [49]. Moreover, the incorporation of Tm_2O_3 significantly enhances the effective electron density of the glass samples. As the Tm_2O_3 content increases, the overall glass density and number of available electrons per unit mass also rise, confirming the potential of Tm_2O_3-doped borotellurite glass as a promising material for gamma radiation shielding applications. According to Table 9, the radiation shielding glass $[(TeO_2)_{70}(B_2O_3)_{30}]_{70}[Bi_2O_3]_{30}$ and $\{[(TeO_2)_{70}(B_2O_3)_{30}]_{75}(Bi_2O_3)_{25}\}_{99}(CeO_2)_1$ in the study by [50] had substantially lower effective electron densities than the 0.030Tm glass sample and thus, proves the effectiveness of suggested glass composition for radiation shielding material.

Table 10. Calculated effective electron density of Tm-doped zinc borotellurite glass using Xcom, Phy-X and NgCal.

Glass Code	Effective Electron Density (for Photons) ($\times 10^{23}$)								
	Xcom			PhyX			NgCal		
	0.662 MeV	1.173 MeV	1.333 MeV	0.662 MeV	1.173 MeV	1.333 MeV	0.662 MeV	1.173 MeV	1.333 MeV
0Tm	2.80324	2.80322	2.80370	3.1984	2.8217	2.7893	2.80315	2.80313	2.80310
0.5Tm	2.80280	2.80280	2.80278	3.1966	2.8209	2.7887	2.80287	2.80290	2.80283
1.0Tm	2.80255	2.80250	2.80263	3.1949	2.8202	2.7880	2.80262	2.80264	2.80256
1.5Tm	2.80194	2.80236	2.80232	3.1931	2.8194	2.7874	2.80231	2.80235	2.80230
2.0Tm	2.80193	2.80196	2.80196	3.1914	2.8187	2.7867	2.80205	2.80206	2.80213
2.5Tm	2.80165	2.80168	2.80166	3.1896	2.8180	2.7861	2.80182	2.80185	2.80177
3.0Tm	2.80140	2.80134	2.80144	3.1879	2.8172	2.7855	2.80157	2.80154	2.80160

According to Table 11, the radiation shielding glass $[(TeO_2)_{70}(B_2O_3)_{30}]_{70}[Bi_2O_3]_{30}$ and $\{[(TeO_2)_{70}(B_2O_3)_{30}]_{75}(Bi_2O_3)_{25}\}_{99}(CeO_2)_1$ in the study by [21] had substantially lower effective electron densities than the 0.030Tm glass sample and thus, proves the effectiveness of suggested glass composition for radiation shielding material.

Table 11. Comparison between the values of the effective electron density of the proposed glass samples and other known shielding materials

Radiation Shielding Material	Effective Electron Density ($\times 10^{23}$)		
	1.173 MeV	1.332 MeV	0.662 MeV
$[(TeO_2)_{70}(B_2O_3)_{30}]_{70}[Bi_2O_3]_{30}$ [21]	-	-	1.8003
$\{[(TeO_2)_{70}(B_2O_3)_{30}]_{75}(Bi_2O_3)_{25}\}_{99}(CeO_2)_1$ [21]	-	-	1.8873
0.3 Tm Using Phy-X (Present Work)	3.1879	2.8172	2.7855
0.3 Tm Using NgCal(Present Work)	2.80157	2.80154	2.80160
0.3 Tm Using Xcom (Present Work)	2.80140	2.80134	2.80144

3.7. Percentage Deviation between Xcom, Phy-X and NgCal

To compare the results of N_{eff} obtained from Xcom, Phy-X, and NgCal, the deviation between the results of MAC, LAC, HVL, MFP, ACS, ECS, $Z_{eff,}$ and N_{el} was calculated. As shown in Table 12, it was found that the comparison of percentage difference for Xcom with respect to PhyX and NgCal with respect to PhyX is very high that is about 14% for MAC, LAC, HVL, MFP, ACS, ECS, $Z_{eff,}$ and N_{el} at energy 0.662 MeV. The high percentage difference is due to different determination methods of ACS, ECS, Z_{eff} and N_{eff} of Phy-X when compared to Xcom and NgCal. The result of

MAC, LAC, HVL, MFP, ACS, ECS, $Z_{eff,}$ and N_{el} for Phy-X was generated from the software directly while Xcom and NgCal results was obtained by calculation mentioned in the methodology section. Thus, there could be different in the decimal point used such as for Avogadro's constant. Also, the mol fraction and weight fraction generated by Xcom, Phy-X and NgCal are significantly different even though similar composition were inserted in each software. This is due to the different database of each software that holds the different information related to reference materials of elements. The result of different reference materials database can be seen by the different MAC value generated by each software. However, significantly very low percentage difference is observed at energy 1.173 MeV and 1.333 MeV that is less than 4%. This concludes that at energy 1.173 MeV and 1.333 MeV more the results are more precise.

Table 12. Percentage deviation of MAC, LAC, HVL, MFP, ACS, ECS, $Z_{eff,}$ and N_{el} calculated of Xcom and NgCal with respect to Phy-X.

Glass Code	Percentage difference of MAC (%)					
	Xcom with respect to Phy-X			NgCal with respect to PhyX		
	0.662 MeV	1.173 MeV	1.333 MeV	0.662 MeV	1.173 MeV	1.333 MeV
0.000Tm	10.06	3.44	2.68	0.53	0.29	0.27
0.050Tm	10.14	3.43	2.70	0.52	0.29	0.27
0.010Tm	10.15	3.45	2.69	0.55	0.29	0.27
0.015Tm	10.12	3.44	2.68	0.52	0.29	0.27
0.020Tm	9.96	3.39	2.65	0.55	0.30	0.27
0.025Tm	9.94	3.37	2.63	0.52	0.30	0.27
0.030Tm	9.85	3.34	2.60	0.55	0.30	0.27
Glass Code	**Percentage difference of LAC (%)**					
	Xcom with respect to PhyX			NgCal with respect to PhyX		
	0.662 MeV	1.173 MeV	1.333 MeV	0.662 MeV	1.173 MeV	1.333 MeV
0.000Tm	10.06	3.44421	2.69418	0.52786	0.29394	0.27297
0.050Tm	10.14	3.42986	2.70064	0.51919	0.28633	0.26562
0.010Tm	10.15	3.45003	2.68850	0.55049	0.29653	0.27351
0.015Tm	10.12	3.43589	2.67645	0.52192	0.28725	0.26629
0.020Tm	9.96	3.38744	2.64579	0.54964	0.29555	0.27255
0.025Tm	9.94	3.37350	2.63391	0.52381	0.28774	0.26658
0.030Tm	9.85	3.34245	2.60342	0.55114	0.29583	0.27267
Glass Code	**Percentage difference of HVL (%)**					
	Xcom with respect to PhyX			NgCal with respect to PhyX		
	0.662 MeV	1.173 MeV	1.333 MeV	0.662 MeV	1.173 MeV	1.333 MeV

0.000Tm	11.16404	3.54507	2.74695	0.52509	0.29308	0.27223
0.050Tm	11.26552	3.52969	2.75377	0.51651	0.28551	0.26492
0.010Tm	11.27423	3.55131	2.74095	0.54748	0.29566	0.27276
0.015Tm	11.22994	3.53615	2.72823	0.51921	0.28643	0.26558
0.020Tm	11.03983	3.48423	2.69588	0.54664	0.29468	0.27181
0.025Tm	11.00935	3.46930	2.68335	0.52108	0.28691	0.26588
0.030Tm	10.89964	3.43606	2.65121	0.54811	0.29495	0.27193

Glass Code	**Percentage difference of MFP (%)**					
	Xcom with respect to PhyX			**NgCal with respect to PhyX**		
	0.662 MeV	**1.173 MeV**	**1.333 MeV**	**0.662 MeV**	**1.173 MeV**	**1.333 MeV**
0.000Tm	11.18765	3.56706	2.76878	0.52509	0.29308	0.27223
0.050Tm	11.28915	3.55168	2.77560	0.51651	0.28551	0.26492
0.010Tm	11.29786	3.57331	2.76277	0.54748	0.29566	0.27276
0.015Tm	11.25357	3.55814	2.75005	0.51921	0.28643	0.26558
0.020Tm	11.06341	3.50621	2.71769	0.54664	0.29468	0.27181
0.025Tm	11.03293	3.49128	2.70516	0.52108	0.28691	0.26588
0.030Tm	10.92319	3.45803	2.67301	0.54811	0.29495	0.27193

Glass Code	**Percentage difference of ACS (%)**					
	Xcom with respect to PhyX			**NgCal with respect to PhyX**		
	0.662 MeV	**1.173 MeV**	**1.333 MeV**	**0.662 MeV**	**1.173 MeV**	**1.333 MeV**
0.000Tm	10.06	3.45	2.70	0.38	0.14	0.12
0.050Tm	10.14	3.43	2.70	0.50	0.27	0.25
0.010Tm	10.15	3.45	2.69	0.69	0.44	0.42
0.015Tm	10.11	3.43	2.67	0.50	0.26	0.24
0.020Tm	9.96	3.38	2.64	0.71	0.46	0.44
0.025Tm	9.93	3.37	2.63	0.49	0.26	0.24
0.030Tm	9.84	3.34	2.60	0.71	0.46	0.44

Glass Code	**Percentage difference of ECS (%)**	
	Xcom with respect to PhyX	**NgCal with respect to PhyX**

	0.662 MeV	1.173 MeV	1.333 MeV	0.662 MeV	1.173 MeV	1.333 MeV
0.000Tm	2.62	2.81	3.18	14.70	0.96	0.22
0.050Tm	2.48	2.81	3.19	14.64	0.93	0.24
0.010Tm	2.43	2.84	3.19	14.62	0.93	0.25
0.015Tm	2.42	2.85	3.19	14.54	0.90	0.27
0.020Tm	2.55	2.81	3.17	14.52	0.89	0.28
0.025Tm	2.54	2.81	3.17	14.44	0.86	0.30
0.030Tm	2.59	2.80	3.16	14.42	0.86	0.30

Glass Code	**Percentage difference of Z_{eff} (%)**					
	Xcom with respect to PhyX			**NgCal with respect to PhyX**		
	0.662 MeV	**1.173 MeV**	**1.333 MeV**	**0.662 MeV**	**1.173 MeV**	**1.333 MeV**
0.000Tm	12.3565	0.6545	0.4954	12.4894	0.8057	0.3436
0.050Tm	12.3194	0.6421	0.5065	12.3302	0.6531	0.4935
0.010Tm	12.2779	0.6252	0.5258	12.1514	0.4798	0.6650
0.015Tm	12.2468	0.6018	0.5403	12.2610	0.6308	0.5095
0.020Tm	12.1984	0.5889	0.5500	12.0555	0.4273	0.7162
0.025Tm	12.1585	0.5714	0.5635	12.1842	0.6015	0.5316
0.030Tm	12.1172	0.5565	0.5815	11.9754	0.3958	0.7428

Glass Code	**Percentage difference of N_{el} (%)**					
	Xcom with respect to PhyX			**NgCal with respect to PhyX**		
	0.662 MeV	**1.173 MeV**	**1.333 MeV**	**0.662 MeV**	**1.173 MeV**	**1.333 MeV**
0.000Tm	12.3551	0.6539	0.5158	12.3578	0.6571	0.4941
0.050Tm	12.3200	0.6424	0.5060	12.3178	0.6386	0.5080
0.010Tm	12.2794	0.6267	0.5239	12.2770	0.6217	0.5214
0.015Tm	12.2500	0.6055	0.5362	12.2387	0.6059	0.5353
0.020Tm	12.2025	0.5937	0.5461	12.1985	0.5899	0.5523
0.025Tm	12.1634	0.5778	0.5582	12.1579	0.5718	0.5622

0.030Tm	12.1234	0.5641	0.5733	12.1182	0.5571	0.5789

4. Conclusion

In this study, the gamma-ray shielding parameters of thulium-doped bismuth borotellurite glasses were systematically evaluated using the Xcom, Phy-X, and NgCal computational platforms. The main objective of this simulation work was to examine how varying thulium oxide (Tm_2O_3) concentrations influence the radiation attenuation performance of $\{[(B_2O_3)_{0.25}(TeO_2)_{0.75}]_{0.75}[(Bi_2O_3)_{0.25}]\}_{1-x}[Tm_2O_3]_x$ glass system. Several key shielding parameters were assessed, including the linear attenuation coefficient (LAC), mass attenuation coefficient (MAC), half-value layer (HVL), mean free path (MFP), effective atomic number (Z_{eff}), and effective electron density (N_{el}). The glass density was found to increase from 6.07 to 6.31 g/cm³ as the Tm_2O_3 concentration increased from 0 to 0.030 mol%. Among all compositions, the 0.030Tm glass exhibited the highest LAC and MAC values across all photon energies, while the undoped 0Tm glass showed the lowest values. A consistent decreasing trend in HVL and MFP was observed with increasing Tm_2O_3 content, indicating enhanced photon absorption efficiency. Furthermore, the 0.030Tm sample demonstrated the highest Z_{eff} and N_{el} values throughout the investigated energy range, confirming the positive influence of Tm_2O_3 on the shielding capability of the glass matrix. The improvement is primarily attributed to the increased glass density and the presence of high-Z elements such as thulium and bismuth, which enhance photon interaction probability. Overall, the simulation results indicate that the 0.030Tm glass exibit enhanced gamma-ray attenuation characteristics compare to other composition studied and may be considered a potential candidate for radiation shielding application. In addition, computational tools such as Xcom, Phy-X, and NgCal are shown to be useful for providing reliable preliminary assessments of glass systems prior to experimental validation.

Declarations

Availability of data and material: The datasets used and analyzed during the current study are available from the corresponding author on reasonable request.

Author contributions: Azuraida Amat conceived and designed the research framework; Nor Falihan Ramli carried out the experimental and computational work; Hasnimulyati Laoding provided critical guidance on the analytical methods and interpretation of results; Nur Arina Mat Rusni performed the data analysis; Wan Yusmawati Wan Yusoff prepared the initial draft of the manuscript. All authors have read and approved the final manuscript. All authors contributed to editorial changes in the manuscript. All authors have participated sufficiently in the work and agreed to be accountable for all aspects of the work.

Acknowledgments: The authors appreciate to Universiti Pertahanan Nasional Malaysia (UPNM) and Universiti Teknologi Mara Pahang (UiTM Jengka) for providing laboratory facilities and equipment used in this study.

Funding: This research was funded by Universiti Pertahanan Nasional Malaysia by Short Term Grant UPNM/2022/GPJP/SG/3 and PS0050 – UPNM/2022/GPPP/SG/14.

Conflicts of interest: The authors declare no conflict of interest.

References

1. Alrowaili, Z.A.; Al-Buriahi, M.S. Gamma absorption/scattering parameters and nuclear radiation shielding performance of AlSN–Zr glass system: Potential use in medical facilities. *Radiation Physics and Chemistry* 2025, 227(2), 112367. https://doi.org/10.1016/j.radphyschem.2024.112367

2. Gerward, L.; Guilbert, N.; Jensen, K.B.; Levring, H. WinXCom – a program for calculating X-ray attenuation coefficients. *Radiation Physics and Chemistry* 2004, 71(3-4), 653–654. https://doi.org/10.1016/j.radphyschem.2004.04.040

3. Şakar, E.; Özpolat, Ö.F.; Alım, B.; Sayyed, M.I.; Kurudirek, M. Phy-X/PSD: Development of a user friendly online software for calculation of parameters relevant to radiation shielding and dosimetry. *Radiation Physics and Chemistry* 2020, 166, 108496. https://doi.org/10.1016/j.radphyschem.2019.108496

4. Gökçe, H.S.; Güngör, O.; Yılmaz, H. An online software to simulate the shielding properties of materials for neutrons and photons: NgCal. *Radiation Physics and Chemistry* 2021, 185, 109519. https://doi.org/10.1016/j.radphyschem.2021.109519

5. AbuAlRoos, N.J.; Baharul Amin, N.A.; Zainon, R. Conventional and new lead-free radiation shielding materials for radiation protection in nuclear medicine: A review. *Radiation Physics and Chemistry* 2019, 165, 108439. https://doi.org/10.1016/j.radphyschem.2019.108439

6. Kavaz, E.; Ekinci, N.; Tekin, H.O.; Sayyed, M.I.; Aygün, B.; Perişanoğlu, U. Estimation of gamma radiation shielding qualification of newly developed glasses by using WinXCOM and MCNPX code. *Progress in Nuclear Energy* 2019, 115, 12–20. https://doi.org/10.1016/j.pnucene.2019.03.029

7. Ibrahim, A.M.; Hammad, A.H.; Abdelghany, A.M.; Rabie, G.O. Mixed alkali effect and samarium ions effectiveness on the structural, optical and non-linear optical properties of borate glass. *Journal of Non-Crystalline Solids* 2018, 495, 67–74. https://doi.org/10.1016/j.jnoncrysol.2018.05.015

8. Al-Buriahi, M.S. Radiation shielding performance of a borate-based glass system doped with bismuth oxide. *Radiation Physics and Chemistry* 2023, 207, 110875. https://doi.org/10.1016/j.radphyschem.2023.110875

9. Larink, D.; Eckert, H. Mixed network former effects in tellurite glass systems: Structure/property correlations in the system $(Na_2O)_{1/3}[(2TeO_2)x(B_2O_3)1 - x]_{2/3}$. *Journal of Non-Crystalline Solids* 2015, 426, 150–158. https://doi.org/10.1016/j.jnoncrysol.2015.07.007

10. Tijani, S.A.; Al-Hadeethi, Y. The influence of TeO2 and Bi2O3 on the shielding ability of lead-free transparent bismuth tellurite glass at low gamma energy range. *Ceramics International* 2019, 45(17), 23572–23579. https://doi.org/10.1016/j.ceramint.2019.08.066

11. Kindrat, I.I.; Padlyak, B.V.; Mahlik, S.; Kukliński, B.; Kulyk, Y.O. Spectroscopic properties of the Ce-doped borate glasses. *Optical Materials* 2016, 59, 20 – 27. https://doi.org/10.1016/j.optmat.2016.03.053

12. Dogru, K.; Aktas, B.; Acikgoz, A. et al. Structural, thermal, and radiation shielding properties of B_2O_3-TeO_2-Bi_2O_3-CdO-Tm_2O_3 glasses: The role of Tm_2O_3. Ceramics International 2024, 50(22): 47384-47394 https://doi.org/10.1016/j.ceramint.2024.09.088

13. Vani. P.; Vinitha, G.; Naseer, K. A. et al. Thulium-doped barium tellurite glasses: structural, thermal, linear, and non-linear optical investigations. *Journal of Materials Science: Materials in Electronics* 2021, 32(18), 23030-23046. https://doi.org/10.1007/s10854-021-06787-5

14. Vani, P.; Vinitha, G.; Sayyed, M. I. et al. Effect of rare earth dopants on the radiation shielding properties of barium tellurite glasses. *Nuclear Engineering and Technology* 2021, 53(12), 4106-4113. https://doi.org/10.1016/j.net.2021.06.009

15. Malidarre, R. B.; Akkurt, I.; Kocar, O. et al. Analysis of radiation shielding, physical and optical qualities of various rare earth dopants on barium tellurite glasses: A comparative study. *Radiation Physics and Chemistry* 2023, 20, 110823. https://doi.org/10.1016/j.radphyschem.2023.110823

16. Yalcin, S.; Aktas, B.; Yilmaz, D. Radiation shielding properties of Cerium oxide and Erbium oxide doped obsidian glass. *Radiation Physics and Chemistry* 2019, 160, 83-88. https://doi.org/10.1016/j.radphyschem.2019.03.024

17. Falihan, R.; Hasnimulyati, L.; Abdul-Manaf, N.A. et al. Effect of thulium oxide on structural, refractive index, and optical band gap of bismuth-boro-tellurite glass system. *Chalcogenide Letters* 2022, 19(10), p715. https://doi.org/10.15251/CL.2022.1910.715

18. Al-Hadeethi, Y.; Sayyed, M.I.; Mohammed, H. et al. X-ray photons attenuation characteristics for two tellurite based glass systems at dental diagnostic energies. *Ceramics International* 2020, 46(1), 251-257. https://doi.org/10.1016/j.ceramint.2019.08.258

19. Sayyed, M.I.; Albarzan, B.; Almuqrin, A. H. et al. Experimental and theoretical study of radiation shielding features of CaO-K2O-Na2O-P2O5 glass systems. *Materials* 2021, 14(14), 3772. https://doi.org/10.3390/ma14143772

20. Teresa, P. E.; Naseer, K. A.; Piotrowski, T. et al. Optical properties and radiation shielding studies of europium doped modifier reliant multi former glasses. *Optik* 2021, 247, 168005. https://doi.org/10.1016/j.ijleo.2021.168005

21. Azuraida, A. Structural, optical and shielding properties of Bi_2O_3/BaO–B_2O_3–TeO_2 doped CeO_2 glass system. Master's Thesis, Universiti Teknologi MARA, 2018.

22. Kumar, P.; Meena, S.S.; Meena, M.; Sharma, N.; Bhatia, B. Structural characterization, raman spectroscopy and FTIR spectroscopy studies of Pr^{3+} doped tellurium bismuth borate glasses. *Journal of Condensed Matter* 2025, 3(1), 103. https://jcm.thecmrs.in/index.php/j/article/view/93

23. Hathot, S.F.; Al Dabbagh, B.M.; Aboud, H. Structural and spectroscopic correlation in barium-boro-tellurite glass hosts: effects of Dy_2O_3 doping. *Chalcogenide Letters* 2024, 21(2), 201–215. https://doi.org/10.15251/CL.2024.212.201

24. Raghvender, R.; Bouzid, A.; Roginskii, E.M.; *et al.* Ab-initio study of structural, vibrational and non-linear optical properties of (TiO_2)-(Tl_2O)-(TeO_2) glasses. arXiv preprint 2025, arXiv:2510.15343. https://doi.org/10.48550/arXiv.2510.15343.

25. Stalin, S.; Edukondalu, A.; Samee, M.A.; et al. Physical and optical investigations of Bi_2O_3-TeO_2-B_2O_3-GeO_2 glasses. *Materials Research Express* 2019, 6(12), 125209. https://doi.org/10.1088/2053-1591/ab689c

26. BN, S.K.; CD; Gedam, R.S. Implications of Ho^{3+}-ions on physical, structural, optical, and spectroscopic features of Na_2O-PbO-borotellurite glass system for feasible applications in optical and laser technology. *Scientific Reports* 2025, 15(1), 28052. https://doi.org/10.1038/s41598-025-13648-2

27. Fausta, D.E.; Marzuki, A.; Cari. Infrared absorption spectra analysis of TeO_2-ZnO-Bi_2O_3-TiO_2 doped B_2O_3 glasses. *Journal of Physics: Conference Series* 2020, 1511, 012076. https://doi.org/10.1088/1742-6596/1511/1/012076

28. Vani, P.; Vinitha, G.; Naseer, K.A.; et al. Thulium-doped barium tellurite glasses: structural, thermal, linear, and non-linear optical investigations. *Journal of Materials Science: Materials in Electronics* 2021, 32(18), 23030–23046. https://doi.org/10.1007/s10854-021-06787-5

29. Clabel H, J.L.; Lozano, G.; Marega Jr, E.; Rivera, V.A.G. XPS analysis of bridging and non-bridging oxygen in Yb^{3+}-Er^{3+}-Tm^{3+}-doped zinc-tellurite glasses. *Journal of Non-Crystalline Solids* 2021, 553, 120520. https://doi.org/10.1016/j.jnoncrysol.2020.120520

30. Sayyed, M.I.; El-bashir, B.O.; Alhuthali, A.M.S.; et al. Gamma radiation shielding and structural features for barium strontium boro-tellurite glass modified with various concentrations of

molybdenum oxide. *Journal of Non-Crystalline Solids* 2021, 559, 120658. https://doi.org/10.1016/j.jnoncrysol.2021.120658

31. Baizura, N.; Yahya, A.K. Effects of Nb_2O_5 Replacement by Er_2O_3 on elastic and structural properties of $75TeO_2-(10-x)Nb_2O_5-15ZnO-xEr_2O_3$ glass. *Journal of Non-Crystalline Solids* 2011, 357(15), 2810–2815. http://dx.doi.org/10.1016/j.jnoncrysol.2011.03.003

32. Azuraida, A.; Nurshahidah, O.; Yusoff, W.Y.W.; et al. Effect of thulium boro-tellurite glass system on radiation shielding parameters. *Journal of Ovonic Research* 2022, 18(2), 141 – 148. https://doi.org/10.15251/JOR.2022.182.141

33. Khanisanij, M.; Sidek, H.A.A. Elastic behavior of borate glasses containing lead and bismuth oxides. *Advances in Materials Science and Engineering* 2014, 2014(1), 452830. https://doi.org/10.1155/2014/452830

34. Lakshminarayana, G.; Sayyed, M.I.; Baki, S.O.; et al. Optical absorption and gamma-radiation-shielding parameter studies of Tm^{3+}-doped multicomponent borosilicate glasses. *Applied Physics A* 2018, 124, 378. https://doi.org/10.1007/s00339-018-1801-4

35. Saudi, H.A.; Tekin, H.O.; Zakaly, H.M.H.; et al. The impact of samarium(III) oxide on structural, optical and radiation shielding properties of thallium-borate glasses: Experimental and numerical investigation. *Optical Materials* 2021, 114, 110948. https://doi.org/10.1016/j.optmat.2021.110948

36. Dwaikat, N.; Sayyed, M.I.; Mhareb, M.H.A.; Dong, M.; Alajerami, Y.S.M.; Alrammah, I.; Khalid, A.; Ashiq, M.G.B. Durability, optical and radiation shielding properties for new series of boro-tellurite glass. *Optik* 2021, 245, 167667. https://doi.org/10.1016/j.ijleo.2021.167667.

37. Rammah, Y.S.; Mutuwong, C.; Yousef, E.S.; Alraddadi, S.; Al-Buriahi, M.S. Gamma-ray/neutron shielding capacity and elastic moduli of $MnO–K_2O–B_2O_3$ glasses co-doped with Er^{3+} ions. *Applied Physics A* 2020, 126, 929. https://doi.org/10.1007/s00339-020-04097-x

38. Bootjomchai, C.; Laopaiboon, J.; Yenchai, C.; et al. Gamma-ray shielding and structural properties of barium–bismuth–borosilicate glasses. *Radiation Physics and Chemistry* 2012, 81(7), 785–790. https://dx.doi.org/10.1016/j.radphyschem.2012.01.049

39. Divina, R.; Marimuthu, K.; Mahmoud, K.A.; et al. Physical and structural effect of modifiers on dysprosium ions incorporated boro-tellurite glasses for radiation shielding purposes. *Ceramics International* 2020, 46(11), 17929–17937. https://doi.org/10.1016/j.ceramint.2020.04.102

40. Serman, N.; Goaz, P.; Pharoah, M. Production of X-rays and Interactions of X-rays with Matter. Columbia University 2000, pp. 11–20.

41. Koirala, B.; Dhobi, S.H.; Khadka, D.; Nakarmi, J.J.N.; Poudyal, K. Study the radiation shielding material of iron oxides on the basis of total cross section. *IOSR Journal of Applied Physics (IOSR-JAP)* 2021, 13(6), 19–25. https://iosrjournals.org/iosr-jap/papers/Vol13-issue6/Ser-2/E1306021925.pdf

42. Al-Buriahi, M.S.; Rashad, M.; Alalawi, A.; Sayyed, M.I. Effect of Bi_2O_3 on mechanical features and radiation shielding properties of boro-tellurite glass system. *Ceramics International* 2020, 46(11), 16452–16458. https://doi.org/10.1016/j.ceramint.2020.03.208

43. Tasnim, A.; Sahadath, M.H.; Islam Khan, M.N. Development of high-density radiation shielding materials containing BaSO4 and investigation of the gamma-ray attenuation properties. *Radiation Physics and Chemistry 2021*, 189, 109772. https://doi.org/10.1016/j.radphyschem.2021.109772

44. Singh, S., Kaur, R., Rani, S., & Sidhu, B. S. Physical, structural and nuclear radiation shielding behaviour of xBaO-(0.30-x) MgO-0.10 Na2O-0.10 Al2O3-0.50 B2O3 glass matrix. *Materials Chemistry and Physics* 2022, 276, 125415. https://doi.org/10.1016/j.matchemphys.2021.125415

45. Aboud, H., Aldhuhaibat, M. J., & Alajermi, Y. Gamma radiation shielding traits of B2O3 – Bi2O3 – CdO – BaO – PbO glasses. *Radiation Physics and Chemistry* 2022, 191, 109836. https://doi.org/10.1016/j.radphyschem.2021.109836

46. Alshamari, A., Mhareb, M. H. A., Alonizan, N., Sayyed, M. I., Dwaikat, N., Alrammah, I., ... & Drmosh, Q. A. Gamma-ray-induced changes in the radiation shielding, structural, mechanical, and optical properties of borate, tellurite, and borotellurite glass systems modified with barium and bismuth oxide. *Optik* 2023, 281, 170829. https://doi.org/10.1016/j.ijleo.2023.170829

47. ALMisned, G., Elshami, W., Issa, S. A., Susoy, G., Zakaly, H. M., Algethami, M., ... & Tekin, H. O. Enhancement of gamma-ray shielding properties in cobalt-doped heavy metal borate glasses: the role of lanthanum oxide reinforcement. *Materials* 2021, 14(24), 7703. https://doi.org/10.3390/ma14247703

48. Al-Hadeethi, Y., Ahmed, M., Al-Heniti, S. H., Sayyed, M. I., & Rammah, Y. S. Rare earth Co-Doped tellurite glass ceramics: Potential use in optical and radiation shielding applications. *Ceramics International* 2020, 46(11), 19198-19208. https://doi.org/10.1016/j.ceramint.2020.04.257

49. Yılmaz, D., Aktaş, B., Yalçın, Ş., & Albaşkara, M. Erbium oxide and Cerium oxide-doped borosilicate glasses as radiation shielding material. *Radiation Effects and Defects in Solids* 2020, 175(5-6), 458-471. https://doi.org/10.1080/10420150.2019.1674301

50. Cheewasukhanont, W., Limkitjaroenporn, P., Sayyed, M. I., Kothan, S., Kim, H. J., & Kaewkhao, J. High density of tungsten gadolinium borate glasses for radiation shielding material: Effect of WO3 concentration. *Radiation Physics and Chemistry* 2022, 192, 109926. https://doi.org/10.1016/j.radphyschem.2021.109926